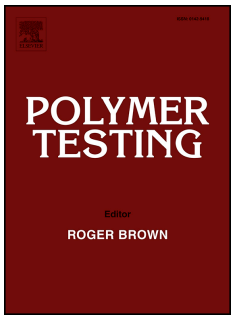

Long-term oxygen plasma etching of UDMA:TEGDMA methacrylate resin: etching rate and physical property changes

Alexandra Borók, Melinda Szalóki, Dávid Gál, Miklós Veres, Attila Bonyár

PII: S0142-9418(25)00046-7

DOI: https://doi.org/10.1016/j.polymertesting.2025.108732

Reference: POTE 108732

To appear in: *Polymer Testing*

Received Date: 2 October 2024

Revised Date: 4 February 2025

Accepted Date: 5 February 2025

Please cite this article as: A. Borók, M. Szalóki, D. Gál, M. Veres, A. Bonyár, Long-term oxygen plasma etching of UDMA:TEGDMA methacrylate resin: etching rate and physical property changes, *Polymer Testing*, https://doi.org/10.1016/j.polymertesting.2025.108732.

Long-term oxygen plasma etching of UDMA:TEGDMA methacrylate resin: etching rate and physical property changes

Alexandra Borók[1,2], Melinda Szalóki[3], Dávid Gál[2], Miklós Veres[2], Attila Bonyár[1,2]

[1] Department of Electronics Technology, Faculty of Electrical Engineering and Informatics, Budapest University of Technology and Economics, Budapest, Hungary

[2] HUN-REN Wigner Research Centre for Physics, Budapest, Hungary

[3] Department of Biomaterials and Prosthetic Dentistry, Faculty of Dentistry, University of Debrecen, Debrecen, Hungary

Abstract

The effect of low-pressure oxygen plasma etching on the physical properties of a dental photopolymer, namely UDMA:TEGDMA in 3:1 weight ratio, was investigated. Samples of the photopolymer were exposed to oxygen plasma from 10 to 120 min time intervals at different power (60, 100 and 140 W) and pressure (0.2, 0.4, and 0.6 mbar) conditions. The etching rate and changes in the surface roughness of the sample were measured with white light interferometry, while the optical properties and chemical changes were monitored by optical and Raman spectroscopy, respectively. It was found that by controlling the power and pressure parameters, steady etching rates can be set up in the 0.11 – 0.48 μm/min range. Longer etching times (e.g. above one hour) were found to increase the surface roughness of the polymer significantly, while reducing its optical transparency. This loss in transparency was successfully restored by depositing a second polymer layer on top of the plasma-etched one. Raman spectroscopy investigations revealed that the degree of conversion, the amount of aromatic molecules and the introduced stress are all depend on the applied etching pressure and power conditions. Actinometry with Ar was performed to measure the internal plasma parameters, and the measured etching rates and observed physical-chemical property changes were correlated with the electron temperature and atomic O densities.

Keywords

acrylates, UDMA, TEGDMA, plasma etching, oxygen plasma, surface roughness, Raman spectroscopy

1. Introduction

Urethane dimethacrylate (UDMA) is a wildly utilized methacrylate resin in dental applications due to its preferable mechanical properties and water-resistance. This monomer can be used alone or in combination with other monomers, like triethylene glycol dimethacrylate (TEGDMA) [1]. While the more viscous UDMA (23.1 Pas [2]) usually serves as the base resin, TEGDMA (0.011 Pas [3]) is frequently used as its diluent comonomer to form a mixture, that has even better properties (better resin strength, less polymerization shrinkage, higher bending strength) than the individual monomers. These materials are usually polymerized by using photo-initiators such as camphoroquinone (CQ) with co-initiators [4] that can be activated by 400–500 nm wavelength blue light [5].

The UDMA:TEGDMA based resin composite is characterized by good mechanical, optical, and layering properties, the latter can be utilized when multi-layered structures with good

adhesion are needed. The thickness of the individual layers can be controlled by additive technologies (spin coating, molding) to a certain extent, but when a precisely defined layer thickness is necessary the application of subtractive technologies, like plasma etching may be required.

UDMA, TEGDMA or bisphenol A-glycidyl methacrylate (BisGMA) based or their mixtures combined with different fillers [6, 7] are commonly used in tooth-colored metal-free post and core restorations next to polymethyl methacrylate (PMMA) posts. The UDMA-based posts are favorable because they have a higher affinity to luting agents than PMMA, and have good bonding adhesion and interaction of hydroxyl groups of stiff dimethacrylates with resin except for surface treatment [8]. During the post manufacturing a superficial polymer rich layer can be found on the surface of it. To obtain sufficient bonding between posts and core build-up resins, different surface treatments are essential like sandblasting, chemical etching, or plasma etching. The plasma treatment improves the adhesion of the polymer and changes the physical and chemical characteristics of the polymer in micrometric and submicrometric scales [9–12]. Moreover, the plasma etching for a suitable period increases the surface roughness of the polymer and even creates groove-like structures. Yavirach et al. tested a UDMA:TEGDMA-based fiber-reinforced post with oxygen plasma treatment [9]. They found that the treatment was more efficient at UDMA-based post than with the argon plasma etched case. The oxygen plasma treatment time altered between a few seconds and 10 minutes, and the effect of longer exposition time was not investigated on a polymer structure.

Generally, plasma treatment can be used to clean and sterilize surfaces with the help of the reactive particles in the plasma [13], but it is also widely applied in the semiconductor industry to develop patterns on substrates. Low-pressure plasma can cause an erosive degradation on the surface, which leads to the dry removal of the material. The effect of plasma etching of different methacrylate resins is scarcely studied in detail in the literature, except for PMMA. The etching rate of PMMA in different conditions is summarized in Table 1. Data corresponding to other acrylate resins from the literature is given in Table 2.

Table 1 *Etching rates of PMMA for different plasmas.*
(ICP – Inductively Coupled Plasma, CCP – Capacitively Coupled Plasma)

Etching rate (nm/min)	Plasma gas	Equipment	Source power (W)	Pres. (mbar)	Gas flow (sccm)	Temp. (°C)	Measurement	Ref.
~60	O_2	Cylindrical Discharge Tube	200	0.75	-	-	Weight loss	[13]
~230	O_2	ICP Plasma Chamber	600	1.77	100	15	Film thickness with ellipsometry	[14]
1500	Ar	ICP Plasma Chamber	600	-	50	-	Thickness	[15]
	O_2				50			
	CF_4				0			
400	Ar		600	-	50	-		
	O_2				40			
	CF_4				10			

200	Ar		600	-	50	-		
	O_2				30			
	CF_4				20			
100	Ar		600	-	50	-		
	O_2				20			
	CF_4				30			
880	O_2	CCP Plasma Chamber	700	-	300	40	Thickness with spectroscopic reflectometer	[16]
829	CO_2							
51.4	CO							
174	XE							
767	O_2	CCP Plasma Chamber	700	-	300	40	Thickness with spectroscopic reflectometer	[17]
521	CO_2							
23	CO							
180	Ar	Plasma Jet	65	-	5000	-	Weight loss	[18]
	O_2				0-50			
110	O_2	CCP Plasma Chamber	50-150	~0.007-0.03	20	-	Thickness with ellipsometry	[19]
20	CF_4							

Table 2 *Etching rates of acrylate resins for different plasmas. (DRM – Dipole Ring Magnet, ICP – Inductively Coupled Plasma, CCP – Capacitively Coupled Plasma)*

Resin type	Etching rate (nm/min)	Plasma gas	Equipment	Source power (W)	Press. (mbar)	Gas flow (sccm)	T (°C)	Measure-ment	Ref.
Polyacrylate ArF resin	350	O_2 (Ar, CF_4)	ICP Chamber	200	~0.07	50	25	Thickness with ellipsometry	[20]
BARC1 (acrylate polymer)	400								
A resist 193 nm acrylate resists	104	C_4F_8	DRM Chamber	1500	-	10	40	Thickness	[21]
		CO				50			
B resist 193 nm acrylate resists	92	O_2				5			
		Ar				200			
PS–b–PDMS	0.98	O_2	CCP Chamber	50-150	~0.007-0.03	20	-	Thickness with ellipsometry	[19]
PDMS–g–PMA-co-PIA	18								
PDMS–g–PMMA	29								
PDMS	1.2								

Based on Table 1, it can be observed that, although the etching rate of PMMA was investigated in every research, the results can vary on a wide range depending on the process gas and the etching parameters as well. As established by our preliminary observations, different etching rates can be produced even if the applied parameters are similar, but a different plasma device is used. The other phenomenon that was commonly described by the authors of these works [17, 22, 23] is how the surface roughness increases, and the refractive index decreases when polymers are exposed to oxygen plasma.

In our previous work [24] we have presented the influence of different gases (Ar, Ar+H, O_2) on the etching rate of UDMA:TEGDMA. Even though oxygen proved to be the most effective gas in this respect, additional research was necessary in order to be able to properly control the thickness of the UDMA:TEGDMA samples. Our main goal here is to present how the different settings of the plasma discharge modify the oxygen plasma etching rate of UDMA:TEGDMA, and also to demonstrate the effect of the oxygen plasma on the surface of the created samples.

2. Materials and methods

2.1. Materials and Sample Preparation

Photopolymerizable dimethacrylate resin mixture was used, which consists of urethane dimethacrylate (UDMA) (Sigma Aldrich Co., St. Louis, MO, USA) and triethylene glycol dimethacrylate (TEGDMA) (Sigma Aldrich Co., St. Louis, MO, USA). 1.5 g UDMA and 0.5 g TEGDMA was weighted and added into a round bottom glass flask. Then the photoinitiator (camphorquinone, CQ, 0.2 m/m%) (Sigma Aldrich Co., St. Louis, MO, USA), along with its co-initiator (ethyl-4-dimethylaminobenzoate, EDAB, 0.4 m/m%) (Sigma Aldrich Co., St. Louis, MO, USA) was dissolved in the 3:1 UDMA:TEGDMA mixture by stirring overnight at room temperature.

To measure the etching rate of the substrate, solid-state layers were created with the help of two glass slides. A few grams of the resin mixture were dropped inside a frame attached to one of the glass slides (Figure 1, a). This frame, prepared by 3D printing from plastic defined the thickness of the initial samples which was usually around 150±5 µm. Then the second glass slide was applied to flatten the polymer droplet (Figure 1; b). This way the material was also protected from the oxygen gas in the surrounding air, as the polymerization process cannot proceed in the presence of oxygen. A standard dental, blue light emitting lamp (Woodpecker LED D, China) was used to accomplish the photo-crosslinking (Figure 1; c). The exposure time was 90 sec in the case of every sample.

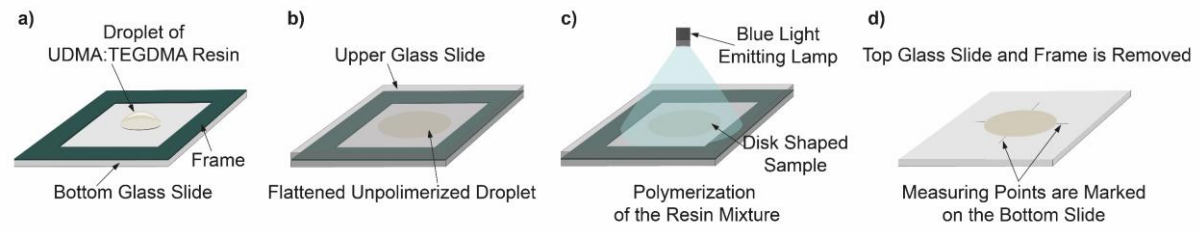

Figure 1 *Schematics of the sample preparation process.*

After the polymerization the top glass slide and the frame were removed, but the prepared sample remained on the bottom glass slide. Otherwise the created UDMA:TEGDMA film can

bend or even roll up due to the thermal effect of the plasma treatment. Measuring the layer's thickness is also more precise this way and with the help of a diamond-headed glass cutter the measurement points can be marked on the glass slide, leaving the samples without impairment (Figure 1; d).

During this research two-layered samples were also created. After preparing the first layer a frame was applied to the bottom glass slide with twice the thickness of the previous frame. A droplet of UDMA:TEGDMA was then placed on the polymerized sample, and was flattened into a disk shape using a second glass slide. After polymerization both the upper glass slide and the frame was removed.

2.2. Plasma Treatment

For the plasma treatment a low-pressure plasma system (Diener, Zepto RIE, Germany) was used. In this research high purity oxygen (99.99%) was applied as process gas. The power output of the chamber was set to 30-50-70%, corresponding to 60-100-140 W. The gas pressure was fixed on three values as well: 0.2 mbar (with gas flow of 2-3 sccm), 0.4 mbar (with gas flow of 11-12 sccm), and 0.6 mbar (with gas flow of 24-26 sccm). The duration of the treatments took a total of two hours for each sample. Each setting included three samples, the treatments of which were divided into different time intervals: one with 10-20-30-30-30 min (five-period) of treatments, one with 60-60 min (two-period) of treatments, and one with 120 min (one-period) of treatment. Within the chamber it was not possible to monitor the temperature of the samples, but considering the time length of the treatments, the temperature in the plasma chamber often noticeably increased. The interruptions of the process, which involved a cooling period, might have affected the results.

2.3. Instrumentation

A white-light interferometer (ZYGO New View 7100) was utilized to measure the thickness of the samples with a 10X objective lens. To have comparable results it was necessary to make measurements always in the same places of each polymer disk. Therefore, the supporting glass slide was marked at four points and these marks were always detected before the measurement. The same equipment was used to determine the surface roughness, for this a 50X objective with scanning length of 40 μm was applied. The results were taken and compared from at least five points of each sample. Later these results were analyzed in Gwyddion 2.65 software and OriginPro 2018 was used for visualization. To get a better understanding of the surface changes further investigation was done with a microscope (Olympus GX53 Inverse Optical Microscope) with a 100X objective. For the cross-sectional view, first a 5-10 nm thick gold nanolayer was evaporated on the surface, to protect it during the mounting process and to help to differentiate the boundaries under the microscope. Then the samples were vertically mounted into an epoxy block which was followed by a grinding and polishing process until the surface roughness was around 40 nm.

Vis-NIR absorption spectroscopy was performed with an Avaspec 2048-4DT spectrometer. An Avantes Avalight DHS halogen light source was used for the measurements, and the spectra were recorded in the 400-1000 nm range with a resolution of 0.28 nm.

For electron temperature measurements and actinometry, the optical emission of the plasma during the treatments with different plasma settings was recorded with an Ocean Optics HR4PRO-XR-ES spectrometer. A 1-meter-long multimode optical fiber (Thorlabs Inc.) was

used to collect the light from the plasma chamber. The bare fiber end was aligned right behind the optical window of the plasma chamber in perpendicular orientation. The window was covered with black shielding cloth to avoid surrounding light entering the fiber. The calibration of the spectrometer was performed with a small neon lamp attached to the other side of the window opposite to the fiber end. For electron temperature determination of the oxygen plasma, we used the Boltzmann curve method with the two sharpest emission lines at 777.33 nm and 844.85 nm. To determine the oxygen atom density, we used actinometry with Ar, where the intensity of the line located at 763.65 nm was compared with the intensity of the line at 844.85 nm. For more information and details regarding actinometry please see the Supplementary Materials.

Raman spectroscopic measurements were performed on a Renishaw InVia micro-Raman spectrometer with 532 nm laser excitation. The excitation was focused into a spot of cca. 2 microns diameter on the sample surface. The spectra were recorded in the 1000-2000 cm^{-1} region with 10 seconds integration time. The baseline correction of the spectra and the fitting of the Raman peaks were performed using the Renishaw WIRE software.

The optical emission of the plasma during the treatments with different plasma settings was recorded with an Ocean Optics HR4PRO-XR-ES spectrometer.

3. Results and discussion

3.1. Etching rate

The main goal of this research was to determine the plasma etching rate of the UDMA:TEGDMA copolymer. A total of three power settings were applied, and three different pressure settings were tested for each power. In Figures 2-4 the etching rates are collected for each experiment. In these figures the etchings rates (v_{t_i}) at every given time point (t_i) are given in a progressive (incremental) manner, as defined by Eq. 1, where h_i is the thickness of the sample measured by white light ellipsometry. For the five-period treatment $t_i = \{0,10,30,60,90,120\}$ min, for the two-period treatment $t_i = \{0,60,120\}$ min and for the one-period treatment $t_i = \{0,120\}$ min. (In other words, at every step the etching rate is calculated by comparing the height of the sample to the previous step, not the initial state.)

$$v_{t_i} = \frac{h_{i-1} - h_i}{t_i - t_{i-1}} \quad (1)$$

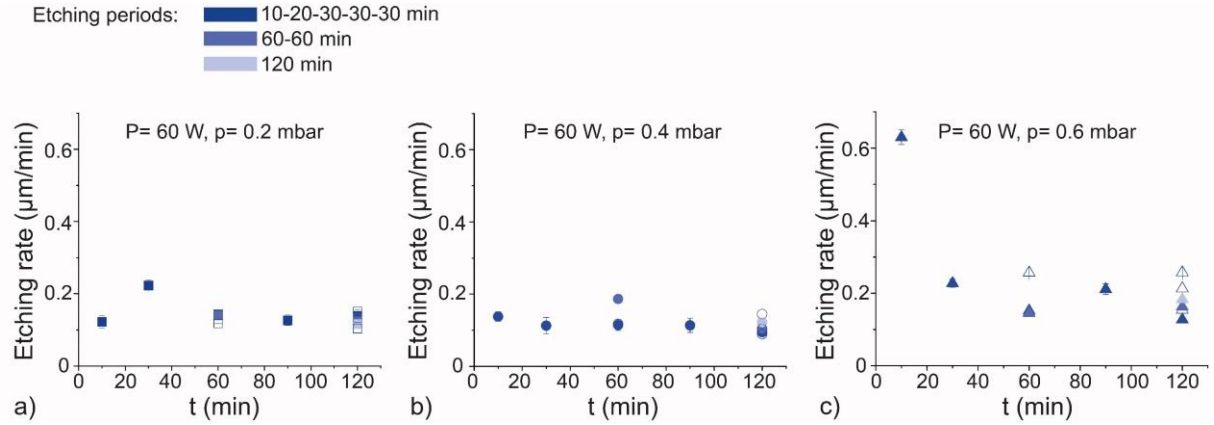

Figure 2 *Etching rate of the plasma treatment of UDMA:TEGMA for 60 W power. The darkest colored results show the results of the five-period treatment, while the lighter belongs to the two-period treatment, and the lightest to the one-period treatment.*

The results belonging to the 60 W power setting can be seen in Figure 2, while Figures 3 and 4 present the etching rates corresponding with the 100 W and 140 W experiments.

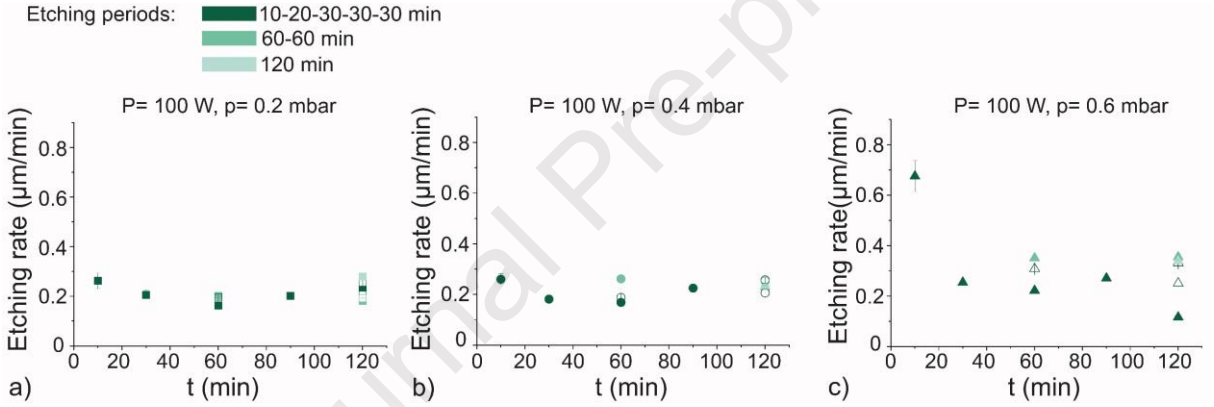

Figure 3 *Etching rates of the plasma treatment of UDMA:TEGMA for 100 W power. The darkest colored results show the results of the five-period treatment, while the lighter belongs to the two-period treatment, and the lightest to the one-period treatment.*

The most important observations that can be made based on the measured trends are the following.

1) The etching rate shows a declining trend in the function of time. In the first 30 min, the etching rate is higher in all cases, then it decreases over time and reaches a quasi-stable or steady-state rate. This effect is more pronounced at some pressure/power combinations. E.g. at high power (at 140 W in Fig. 4) all curves show a steep drop after 10 min etching, while at lower powers (60 and 100 W in Figs. 2-3) only the curves measured at 0.6 mbar show this steep decline.

2) Both the initial etching rate (measured after the first 10-minute etching) and the steady-state etching rate increase noticeably with the increasing power (at a fixed pressure setting), while the steady-state etching rate increases only slightly with the increasing pressure at a fixed power.

3) The etching rates obtained by the five-period treatments are usually lower than the ones obtained by the two- and one-period treatments at the same time point. This is caused by the

declining trend of the etching rate and the way of calculation (see Eq. 1). For example, in the case of the data points at 120 min, the one-period etching rate is calculated by comparing to the initial height (at 0 min, thus it takes into account the initially higher etching rate as well), while the five-period treatment is calculated based on the heights measured at after 90 min and 120 min points (see Eq. 1).

4) As mentioned in the experimental section, longer treatments can cause a noticeable (couple of 10°C) increase in the temperature of the samples, which might also cause variation by comparing the longer etching times (60 min, 120 min) with the shorter periods containing interruptions and cooling times between the cycles. The effect of possible heating will be discussed in Section 3.5., in the light of the observes chemical changes measured with Raman spectroscopy.

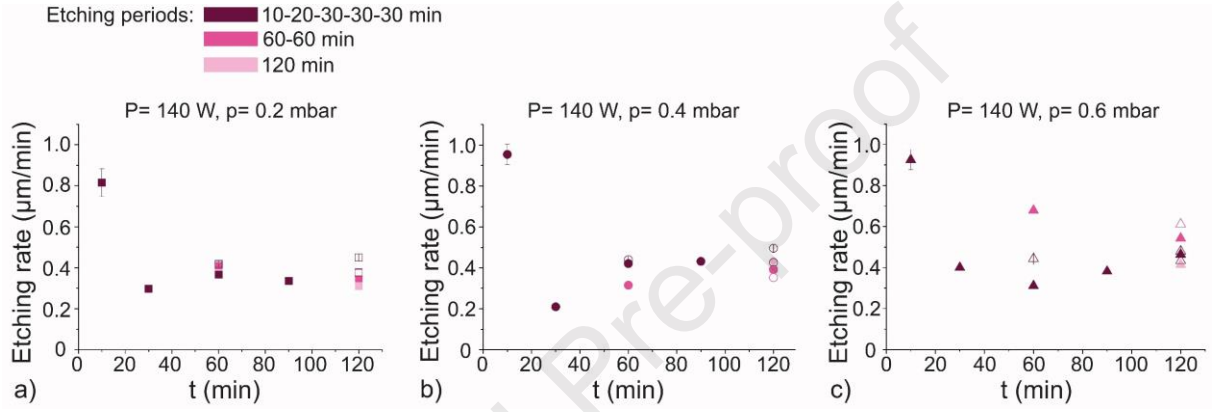

Figure 4 *Etching rate of the plasma treatment of UDMA:TEGMA for 140 W power. The darkest colored results show the results of the five-period treatment, while the lighter belongs to the two-period treatment, and the lightest to the one-period treatment.*

For the sake of better understanding the effect of plasma parameters on the etching rate a cumulative etching rate ($\overline{v_{t_i}}$) was calculated on the dataset obtained by the five-period etching, as in Eq. 2.

$$\overline{v_{t_i}} = \frac{h_0 - h_i}{t_i - t_0} \tag{2}$$

Here the thickness of the sample at a given time (h_i, t_i) is always compared to the initial state ($h_0, t_0 = 0\ min$). An example for the resulting characteristics is given in Fig. 5, where the three pressure setups are compared for the 140 W power case.

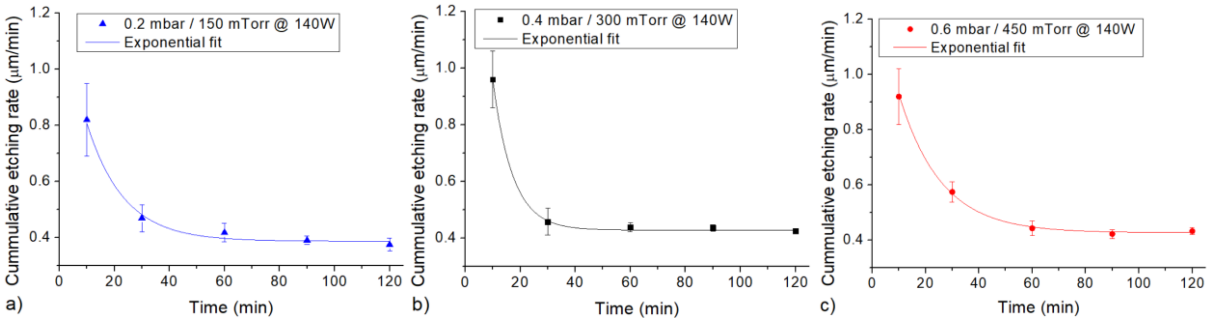

Figure 5 *Cumulative etching rate (see Eq. 2) of the plasma treatment of UDMA:TEGMA measured at 140 W power for the three investigated pressures. The datasets were fitted with an exponential decay equation (see Eq. 3).*

The exponentially decaying characteristic of the etching rate is even more apparent in Fig. 5. The results are fitted with a standard decay equation (Eq. 3) to obtain the steady-state etching rate (v_{ss}), where A and c are fitting parameters.

$$v = Ae^{-\frac{t}{c}} + v_{ss} \tag{3}$$

The resulting steady-state etching rates are given in Table 3, along with the rates calculated for the initial 10-minute etching.

Table 3 *The etching rates of UDMA:TEGDMA at different experimental conditions, based on the five-period treatments. Data is given for both the initial 10-minute etching period and the steady-state etch, as defined in the text.*

Initial 10-minute etching (± based on 4 measurements)			
Plasma pressure, mbar	**Etching rate, µm/min**		
	Plasma power, W		
	60	***100***	***140***
0.2	0.12±0.03	0.26±0.06	0.82±0.13
0.4	0.14±0.03	0.26±0.04	0.96±0.10
0.6	0.63±0.04	0.68±0.12	0.92±0.10
Steady-state etching from exponential fit			
Plasma pressure, mbar	**Etching rate, µm/min**		
	Plasma power, W		
	60	***100***	***140***
0.2	0.14	0.20	0.39
0.4	0.12	0.20	0.43
0.6	0.22	0.27	0.43

The results in Table 3 support our previous observations, however, the etching rate increase is noticeably not always monotonous in the function of the pressure or power increase. This will be investigated in more detail in the next chapter.

3.2. Etching rate in the function of the internal plasma discharge parameters

In order to understand the effect of the considered external engineering parameters (pressure and power) on the etching rates we obtained the internal plasma discharge parameters (electron temperature and radical number density) for the investigated oxygen plasmas. These internal plasma parameters directly correlate with induced physical-chemical changes in the material [25]. Besides, since the ion density and energy strongly depend on the external parameters, which may strongly vary between different instruments, knowing the internal parameters is also essential for the sake of reproducibility.

The detailed methodology to obtain the internal plasma parameters with optical spectroscopy is discussed in the Supplementary Materials section. The obtained electron temperatures are also compared with other published results measured on similar oxygen plasmas here.

In short, we first obtained the electron temperature of the generated plasmas, by using the Boltzmann curve method, based on [26-29]. Subsequently we determined the oxygen atom density (n_O) with actinometry using 5% Ar in the oxygen plasma, based on [30-32]. At 0.2 mbar the plasma equipment (Diener Zepto) could not maintain the Ar and O_2 flow rates required for the 5% Ar ratio. Thus, in this case only the electron temperature was determined based on clean oxygen plasmas. The resulting electron temperatures and O densities in the function of the external (power, pressure) parameters are presented in Fig. 6, while the etching rates are correlated with the internal parameters in Figs. 7 and 8.

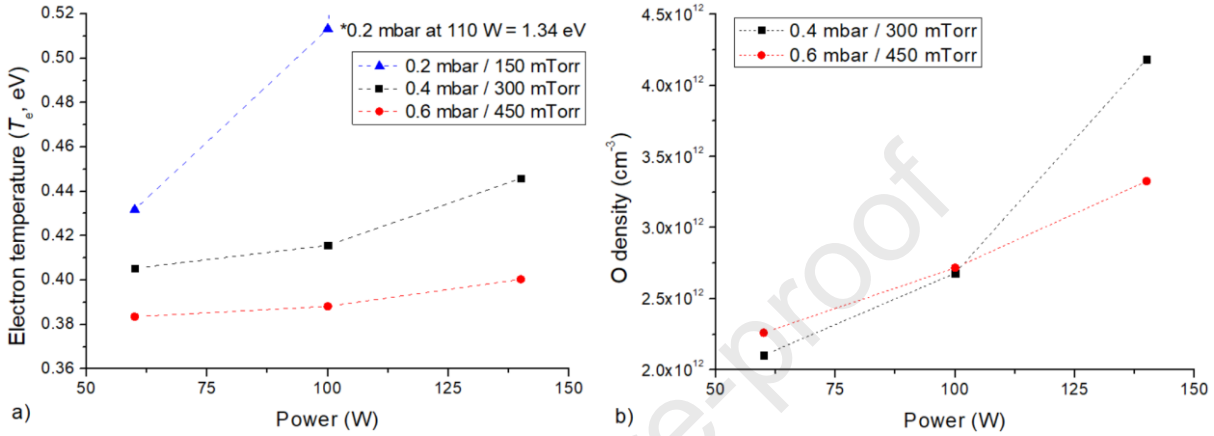

Figure 6 *The electron temperatures (**a**) and O densities (**b**) in the function of the applied pressure and power parameters.*

As can be seen, both the electron temperature and O density increase with increasing power, and the electron temperature also has a clear negative correlation with the applied pressure, consistent with other works using actinometry to measure plasma parameters [30]. However, there is no clear correlation between the O density and the pressure. Interestingly at 140 W power the O density is higher at 0.4 mbar than at 0.6 mbar. This is not a measurement error. As can be seen in the Supplementary Materials section there is a strong negative correlation between the pressure and the n_O/n_{O_2} ratio, consistently with other reports working in the same pressure range [32], but taking into consideration the density of molecular oxygen in the chamber, we get the characteristics presented in Fig. 6 b).

By comparing Figures 7 and 8 we can see that although both the initial and the steady-state etching rate correlates with both the electron temperature and the O density, the absolute pressure still modulates the results. At a given pressure increasing the electron temperature (which can be directly related to the peak energy of the ion energy distribution function, IEDF [33]) increases both the initial and the steady-state etching rates (Fig. 7).

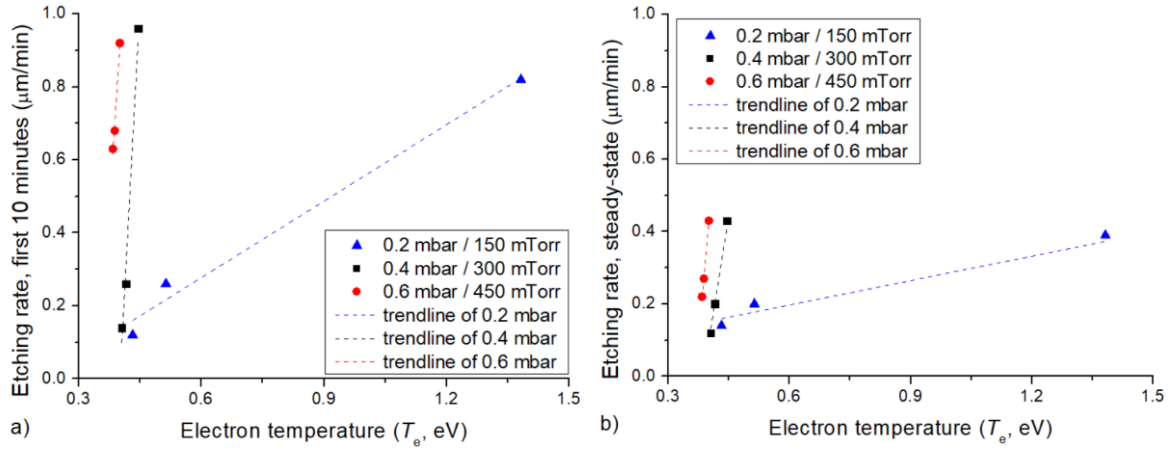

Figure 7 *Etching rates in the function of the electron temperatures. (**a**) Etching rate calculated in the first 10 minutes of etching; (**b**) steady-state etching rate (see definition in the text and Table 3). The trendlines are linear fits of the corresponding data.*

The etching rates also increase with the density of oxygen in the plasma. The correlation is especially nice for the steady-state case (Fig. 8 b), where the slope of the two trendlines corresponding with the two pressures coincide within the experimental uncertainties. By comparing Fig. 8 a) and b) we can also see that in the first phase of the etching the rate is more sensitive to the O density (the characteristics are steeper), compared to the later stages.

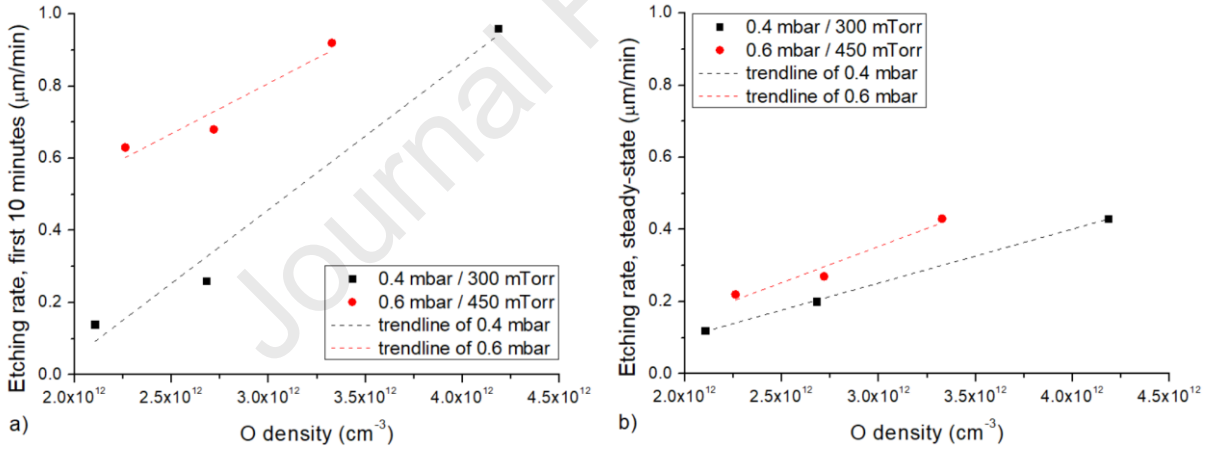

Figure 8 *Etching rates in the function of the O density. (**a**) Etching rate calculated in the first 10 minutes of etching; (**b**) steady-state etching rate (see definition in the text and Table 3). The trendlines are linear fits of the corresponding data.*

In the next sections the physical and chemical properties of the etched samples will be investigated and discussed in comparison with the external and internal parameters of the plasma discharge.

3.3. Surface roughness

To investigate the changes in the surface physical properties, the samples of two-period treatment were examined with microscopy. In Figure 9 b) the image of an untreated sample can be seen. This picture presents well how transparent the polymerized samples are and (except for major surface injuries or bubbles) it is almost impossible to create a representative picture

of the surface with a microscope. Thus, we investigated the surfaces with a white-light interferometer (ZYGO New View 7100) and calculated the surface roughness of the treated samples according to Eqs. 4 and 5, where $\{z_i, i = 1,\ldots,N\}$ are the height of the individual scanned points on the surface.

$$S_a = \frac{1}{N}\sum_{i=1}^{N}|z_i| \tag{4}$$

$$S_q = \sqrt{\frac{1}{N}\sum_{i=1}^{N} z_i^2} \tag{5}$$

The surface roughness in this initial state is S_q=0.9±0.1 nm, S_a=0.6±0.1 nm on a 100×100 μm^2 area. The microscopic images of the plasma-treated samples are more comparable if arranged not according to the applied power but to the applied pressure. Thus, in Figure 10 and Figure 11 the results of the treatments at 0.2 mbar, 0.4 mbar and 0.6 mbar pressure can be seen respectively. In all cases there was a visible difference not just between the reference image (Figure 9 b), but between the one-hour (Figure 10) and two hours (Figure 11) etching as well. It can also be seen that increasing the power of the plasma chamber results in a greater change in the surface even on a microscopic level. In Figure 12 the cross-sectional views of the samples can be seen, where it is detectable that the depths of these changes can even reach several microns. Figure 9 a) shows a schematic image of this phenomena. Further analysis of the formed surface structures was then performed with a white light interferometer instead of a microscope.

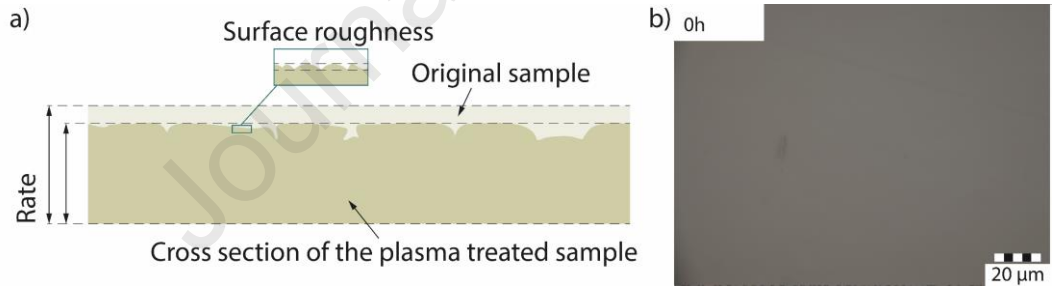

Figure 9 *a) Schematic illustration of the changes in the surface roughness of the photopolymers after plasma etching. b) Optical microscopy image of the untreated sample.*

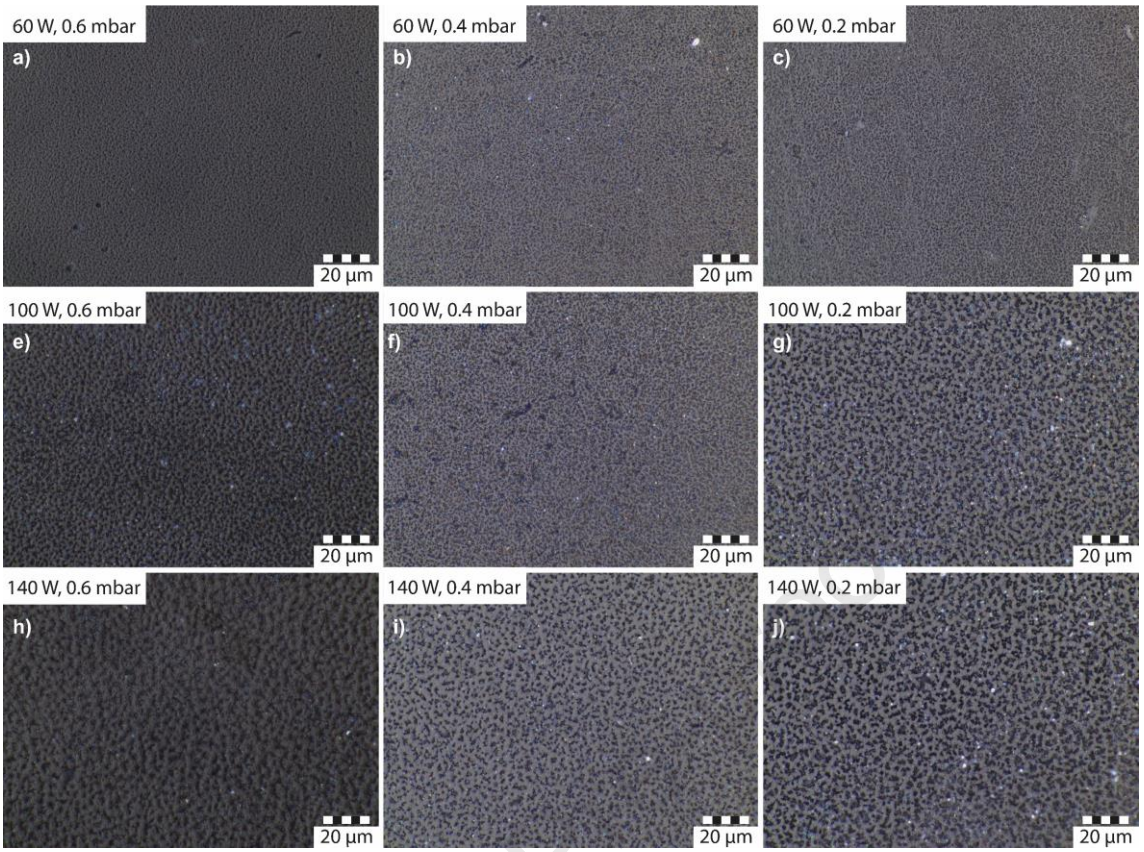

Figure 10 *Optical microscopy images of samples after 1 hour of plasma treatment with different power and pressure conditions.*

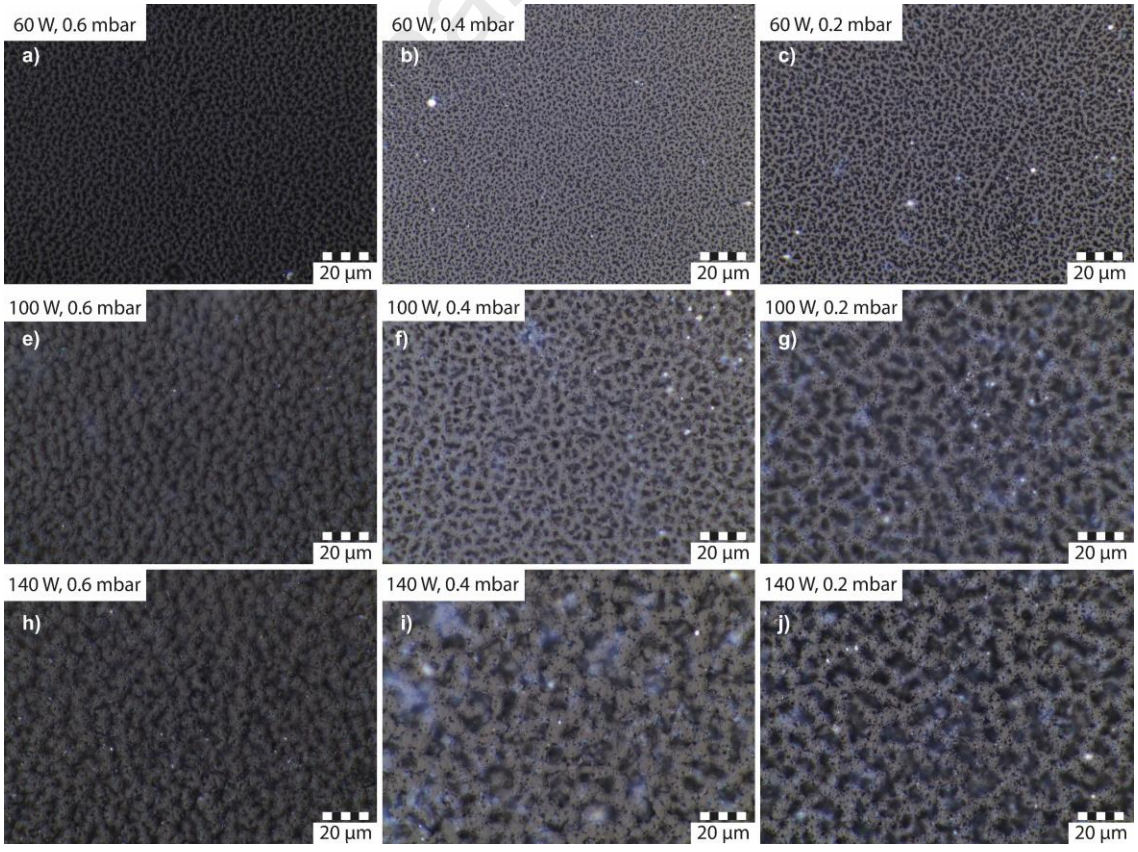

Figure 11 *Optical microscopy images of samples after 2 hours of plasma treatment with different power and pressure conditions.*

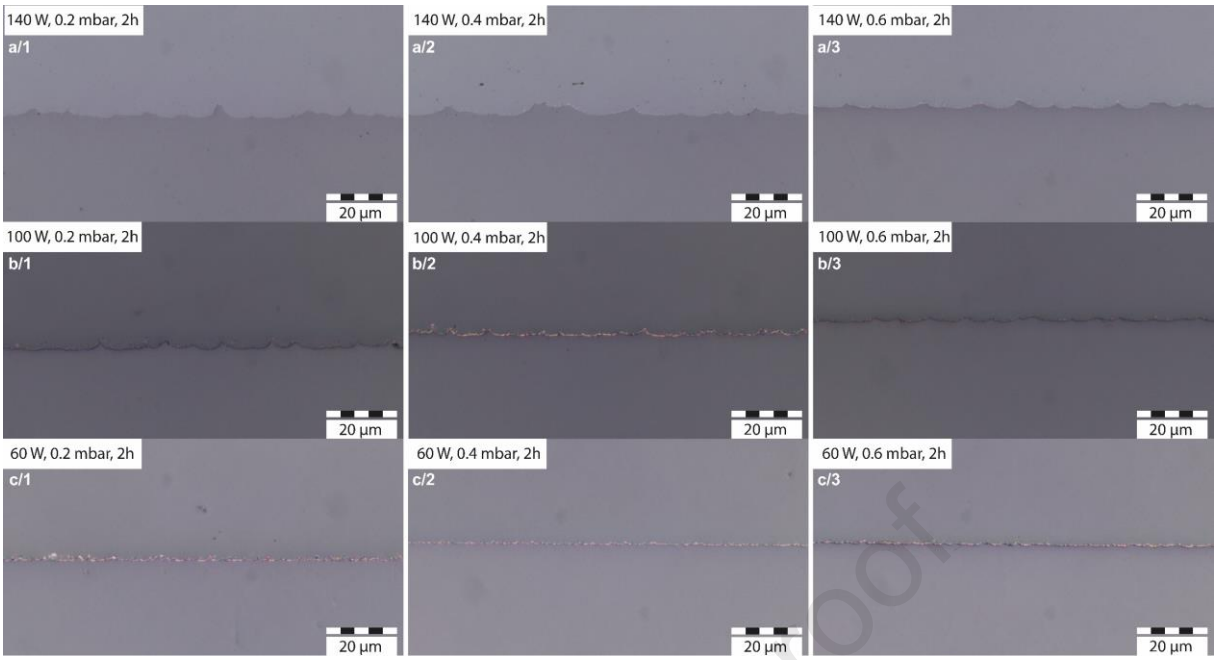

Figure 12 *Cross-sectional view of the cold mounted, gold coated samples after plasma treatment.*

In Figure 13 the results of the surface roughness measurements are presented with RMS roughness (S_q) and mean roughness (S_a) on a 100×100 µm^2 area. As the applied pressure decreased the surface roughness increased in the long term, the two hours treatments showed higher values in the case of 100 W and 140 W settings with 0.4 mbar (140 W S_q > 1 µm) than with 0.6 mbar (140 W S_q ~800 nm). The results for 0.2 mbar are not presented here as the white light interferometer could not measure the surface inequalities properly in that case.

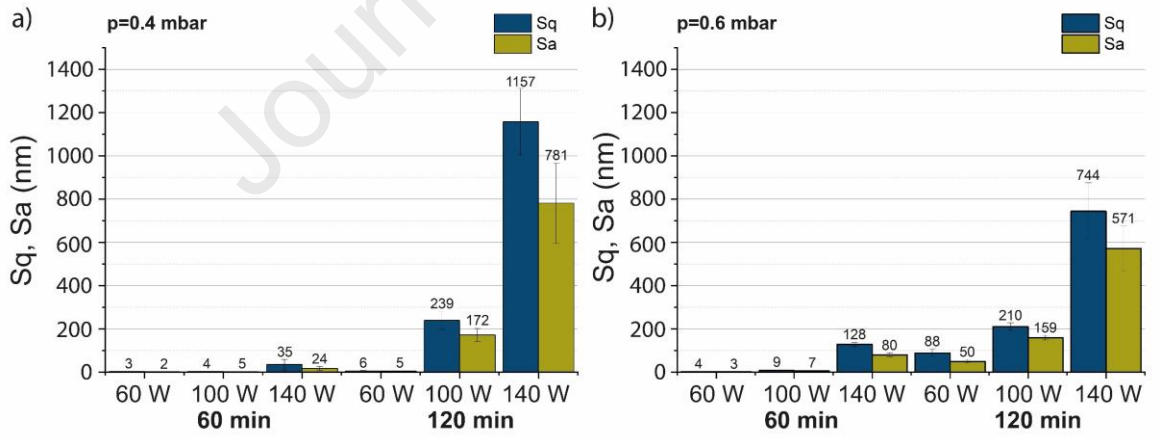

Figure 13 *Result of surface roughness measurements with white light interferometry on a 100×100 µm^2 area for a) 0.4 mbar and b) 0.6 mbar plasma pressures. With blue the S_q while with green S_a is presented.*

In Fig. 14 the surface roughness (S_a) measured after 120 min exposure is plotted against the electron temperature and O density parameters. As can be seen there is a direct correlation between the obtained surface roughness and the O density in the plasma (Fig. 14 b), confirming that this parameter is the most important in determining the roughness of the samples after etching. Considering that based on Figs. 10 and 11 samples etched in 0.2 mbar have the highest

roughness and we can presume that at this pressure the O density is higher at the respective powers.

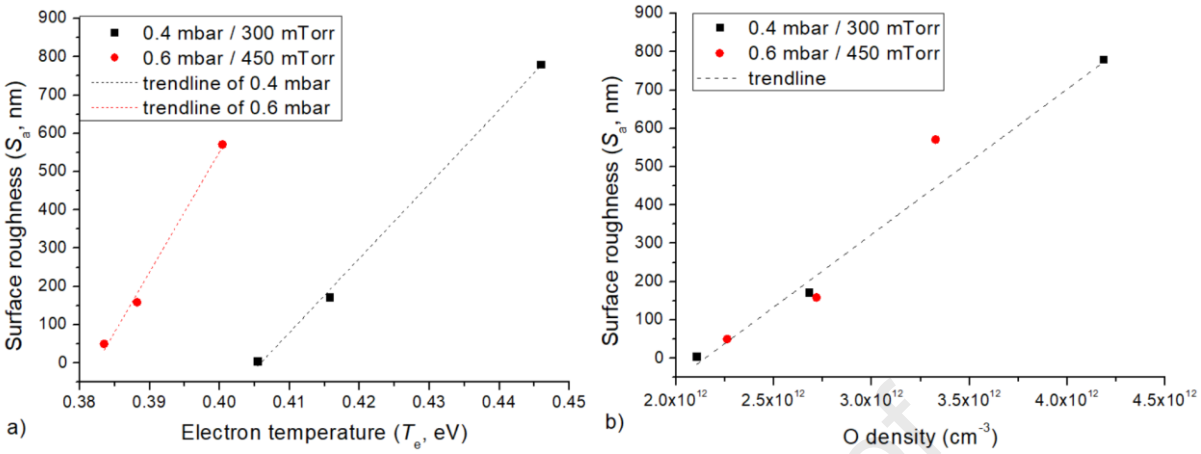

Figure 14 *Correlation between the surface roughness (S_a, after 120 min etching) with the electron temperature and O density parameters of the used plasmas.*

The increasing surface roughness during etching can be one of the reasons behind the exponentially decreasing etching rate (see Fig. 5). But it has to be mentioned that the exponential etching rate is possibly a result of more complex processes caused by the plasma, including changes in the surface energy of the polymer [38], changes in the degree of conversion (see Section 3.5 Chemical properties) and also temperature effects in the case of longer etching times performed in one run.

By comparing the relationships between the obtained etching rates, surface roughness and the plasma parameters we can see that although the process naturally depends on the ion energies (directly related to the electron temperature [33]), the clear correlation with the O density (especially in the case of surface roughness) shows that the density of reactive neutrals is the principal parameter of the etching process. This observation corresponds well to previous studies, where they found that the presence of oxygen atoms significantly increases the etching process in acrylates compared to pure argon plasmas, where physical sputtering by ions is the main mechanism of etching [39]. Oxygen atoms enhance the etching rate, because carbohydrates in polymers are easily volatized in the presence of reactive oxygen [39], forming CO, CO_2, HO, and H_2O molecules as products [40]. The reason for increased surface roughness – and for the dependence of surface roughness on the oxygen concentration – can be explained by the etching selectivity of the components of our composite material [40], namely the different probability for oxidation with O atoms in the cases of UDMA and TEGDMA. The development of surface roughness is affected by many other factors, such as chemical inhomogeneity (e.g. inhomogeneity in the degree of polymerization, void fraction etc.) or etching inhibitors on the surface of the polymer [41]. As in our Diener Zepto RIE system the electrode is exposed inside the plasma chamber, we can also assume the presence of sputtered alumina particles on the surface, which can act as etching inhibitors and thus as nano- or micro-masks during etching [42]. More, in-depth investigations would be needed to discern the effect of these factors on the developed roughness pattern.

3.4. Optical properties

During this research it was also noticed that the transparency of the samples changes as the etching progresses; the completely transparent samples lose this quality after 2 hours of treatment for all parameter combinations (Figure 15).

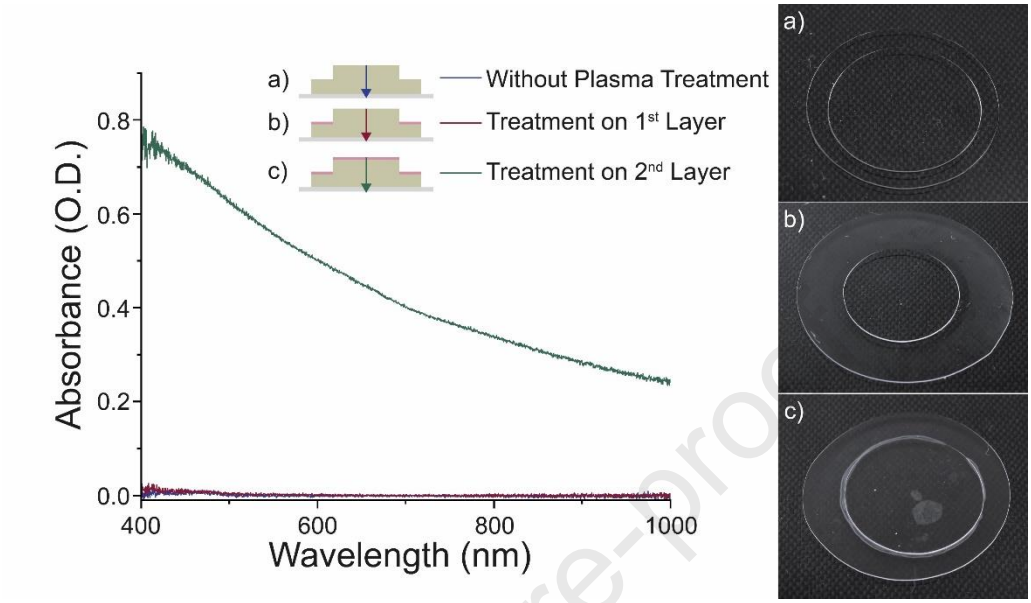

Figure 15 *(Left) Absorbance of the UDMA:TEGMA sample before and after a two-layer 100 W, 60 mbar plasma treatment. (Right) Photo of two-layered UDMA:TEGMA samples, a) two layers without plasma etching treatment, b) bottom layer with, top layer without plasma etching treatment c) two layers with plasma etching treatment.*

In Figure 15 while image a) shows that the samples are transparent after the polymerization, and even with stacking, this quality does not change, in Figure 15 c) it is visible that how the transparency decreased due to the plasma etching treatment. In Figure 15 b) it was demonstrated that even though the first layer lost its transparency after etching, adding and polymerizing a second layer on the top of the first, the sample's transparency is comparable to the one in Figure 15 a). Must be mentioned that in Figure 15 b) around the perimeter of the top layer we can observe a ring with a lighter shade that is due to the fact that the UDMA:TEGDMA polymer cannot polymerize if oxygen is in the surrounding area, as it was mentioned before. This means there is some left over unpolymerized material next to the second layer because of the sample preparation arrangement, which could be removed after polymerization.

The changes in color are purely of mechanical origin. As it was shown previously the surface roughness of the samples increases as a result of the plasma treatment, which is typical for methacrylates [17, 22]. This assumption is also supported by Figure 15 b), as the second applied layer can fill up the inequalities of the surface, restoring the sample to its original transparency. Finally, the Raman spectroscopy investigations did not find any chemical changes which could be accounted for color changes, as it will be discussed in the next section.

3.5. Chemical properties

The Raman spectra of the samples etched with different powers at 0.2 mbar pressure, together with the untreated one are shown in Figure 16. They are normalized to the intensity of the 1460 cm^{-1} peak, related to C–H deformation vibrations of the CH_3 groups of the methacrylate backbone [34]. Similar spectra were recorded on the 0.4 mbar and 0.6 mbar samples.

The spectra contain the characteristic Raman bands of the UDMA:TEGDMA mixture and the residual photoinitiator. Their detailed assignment can be found in [35], and also in Table 4. The effect of plasma etching can be observed mainly on the changes in the 1605, 1638 and 1715 cm^{-1} bands. In the following, these peaks will be analyzed in detail.

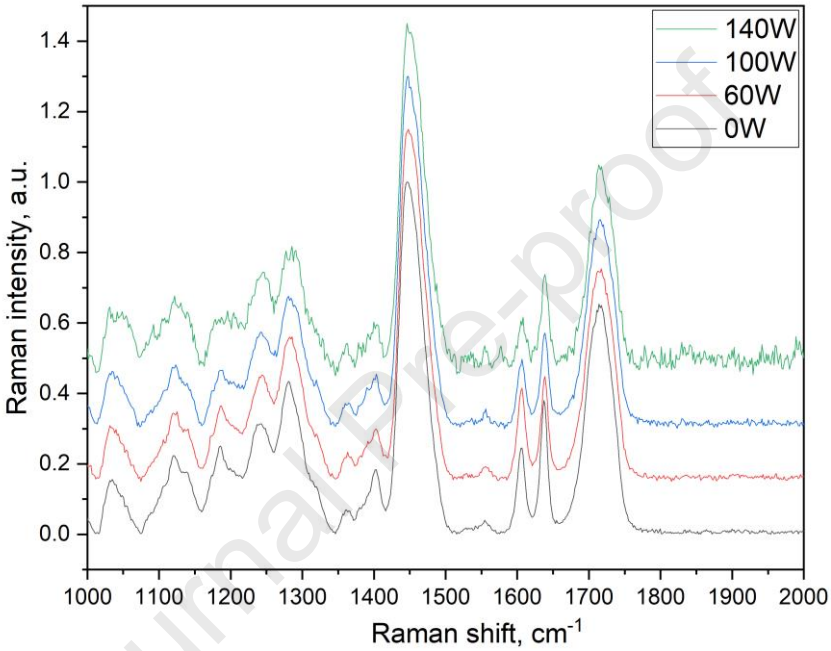

Figure 16 *Raman spectra of the untreated (0 W) and plasma etched with different plasma powers at 0.2 mbar pressure UDMA:TEGDMA surfaces.*

The 1605 cm^{-1} Raman peak is related to aromatic C=C vibrations. In the present system the two monomers, UDMA and TEGDMA, as well as the CQ initiator contain no aromatic ring. Therefore, this peak can solely be attributed to the EDAB co-initiator molecules being entrapped in the highly cross-linked polymer matrix. The change of the peak position and intensity with plasma pressure and power are shown in Figure 17. It can be seen that the plasma etching causes a peak shift to higher wavenumbers. The highest change in the band position can be observed for the 60 W and 0.2 mbar plasma conditions. With further increase of the pressure the change in the peak position is less prominent. On the other hand, the intensity of the peak decreases, especially in the structures obtained with 0.4 and 0.6 mbar pressures. The highest drop belongs to 140 W power.

Table 4. *Assignment of the main Raman peaks observable in the spectra of the UDMA:TEGDMA samples.*

Raman peak, cm^{-1}	Assignment
1033	C-O stretch (TEGDMA, UDMA)
1122	CH_2 twist (TEGDMA, UDMA)
1185	C-H bend (EDAB)
1242	C-O stretch (TEGDMA, UDMA)
1280	C-O stretch (TEGDMA, UDMA)
1402	C-CH2 (UDMA)
1445	C-C + $C-H_2$ stretch (TEGDMA, UDMA)
1605	C=C stretch (EDAB)
1638	C=C stretch (TEGDMA, UDMA)
1715	C=O stretch (TEGDMA, UDMA)

The lowering of the Raman band intensity indicates the decrease of the number of aromatic rings in the plasma etched regions of the polymer. This can be due to the 1) removal of the EDAB from the structure by the ion bombardment and/or heating and 2) damage and destruction of the entrapped EDAB molecules by the ion bombardment. The peak shift, on the other hand, indicates increased internal stress in the plasma treated regions of the polymer. This can be attributed to remarkable structural changes in the matrix, supporting the distortion and destruction of the co-initiator molecules by the plasma treatment.

As it has been shown earlier, the higher the plasma pressure, the higher the (initial and steady-state) etching rate. As the Raman results for the 1605 cm^{-1} band show, the increase of the etching rate is accompanied with lower internal stress in the polymer structure, but also with a lower amount of the entrapped molecules.

The dependence of these Raman peak parameters on internal plasma parameters is shown in Figs. S7 and S8 of the Supplementary Materials section. It can be seen that (except in the 0.2 mbar/140W case) the peak position (internal stress) rapidly decreases, and the peak intensity (amount of entrapped EDAB molecules) rapidly increases with the electron temperature. On the other hand, both parameters decrease with the oxygen density.

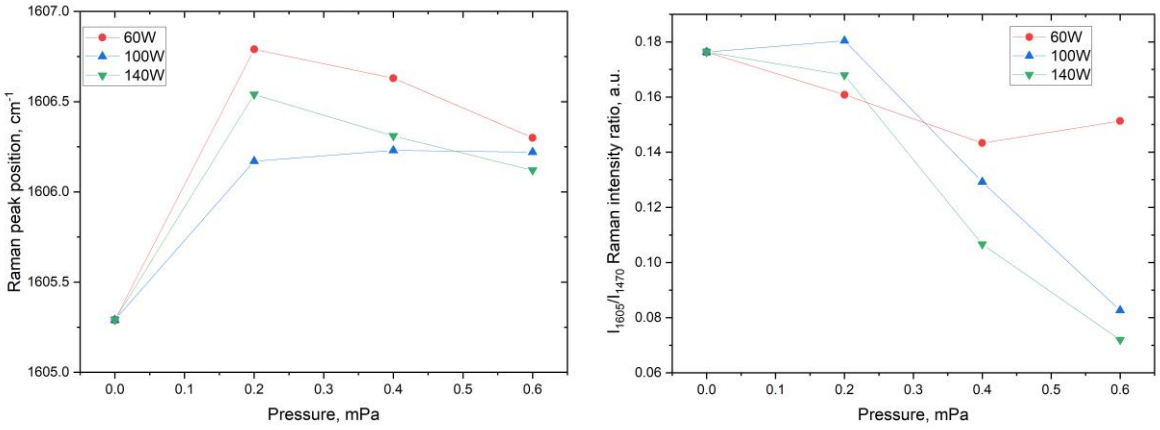

Figure 17 *Change of the position (left) and the relative intensity (right) of the 1605 cm^{-1} Raman peak with plasma pressure for different powers.*

The 1638 cm^{-1} Raman peak in the spectrum belongs to the C=C vibrations of the vinyl group on the methacrylate monomers. The polymerization is realized through the braking of this double bond leading to the formation of interconnections between the monomers. Both UDMA and TEGDMA are dimethacrylates, therefore, instead of chains their polymers consist of highly crosslinked structures. The breaking of the double bonds and the decrease of the corresponding Raman peak intensity can be used to monitor the degree of polymerization in these materials [34].

As Figure 18 shows, both the peak position and the relative intensity of the 1638 cm^{-1} Raman peak are affected by the plasma etching. The Raman band shifts to higher wavenumbers by more than 1 cm^{-1} in all cases. This shift is almost independent of the plasma power, and slightly increases with the plasma pressure. The bond intensity increases with pressure up to 0.4 mbar for 60 W power, then it returns to a value being close to that of the untreated sample. For 100 W and 140 W powers, however, it decreases with the pressure.

From the above changes the peak shift indicates the increase of the internal stress of the plasma etched structure. This is in good agreement with the behavior of the Raman peak of the entrapped (chemically unbound) co-initiator. The intensity changes, however, are different for the 60 W and 100 W and 140 W cases. For 60 W the number of C=C double bonds increases, meaning the decrease in the level of crosslinking (degree of polymerization) of the polymer. This behavior is less pronounced for higher plasma pressures. At higher plasma powers, on the other hand, the treatment results in increased crosslinking of the polymer network in the treated region, indicating the formation of a more crosslinked polymer structure because of the treatment.

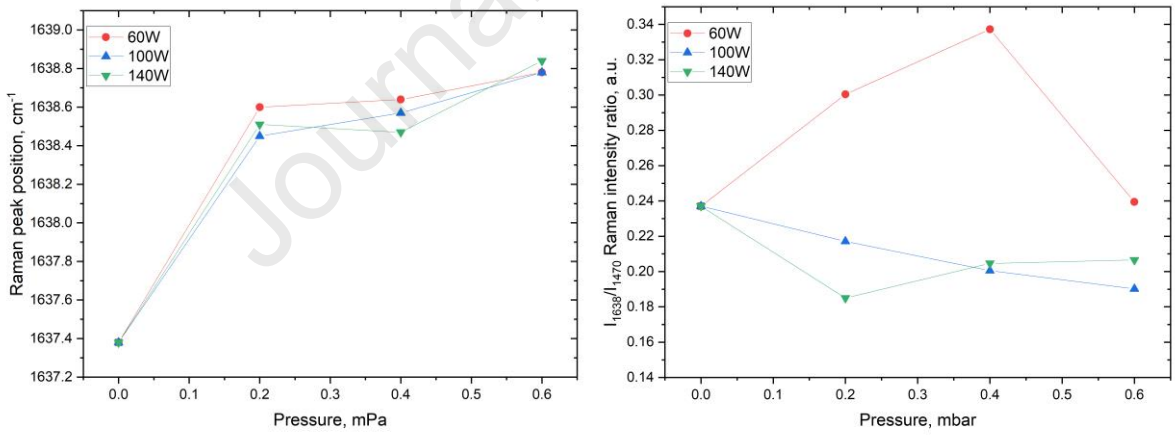

Figure 18 *Change of the position (left) and the relative intensity (right) of the 1638 cm^{-1} Raman peak with plasma pressure for different powers.*

A similar behavior can be observed for the 1715 cm^{-1} Raman band that can be assigned to the carboxyl (C=O) bond of the methacrylate group (Figure 19). This strong bond is not breaking during the polymerization, but its Raman activity is dependent on the conjugation with the neighboring C=C bond described above (the 1638 cm^{-1} Raman peak). Due to this, the C=O peak intensity decreases as the number of conjugated C=O bonds lowers during the polymerization. However, the C=O groups of the formed polymer network will have their own Raman scattering contribution slightly shifted to higher wavenumbers due to the lack of conjugation.

As Figure 19 shows, the C=O peak shifts to higher wavenumbers, and, based on the findings described above, this can be attributed to two factors: the increase of internal stress due to structural changes and the higher degree of crosslinking [24,34,36]. A similar behavior has been observed earlier during the Raman spectroscopic study of the degree of conversion of another methacrylate-based polymer [37]. As it was shown, the degree of polymerization decreases in samples treated with 60 W plasma power and this behavior can be observed for the intensity of the C=O band as well. And it also appears in the peak shifts as they are the smallest in the 60 W samples. The trends for the other two plasma powers are also in good agreement with those of the C=C band.

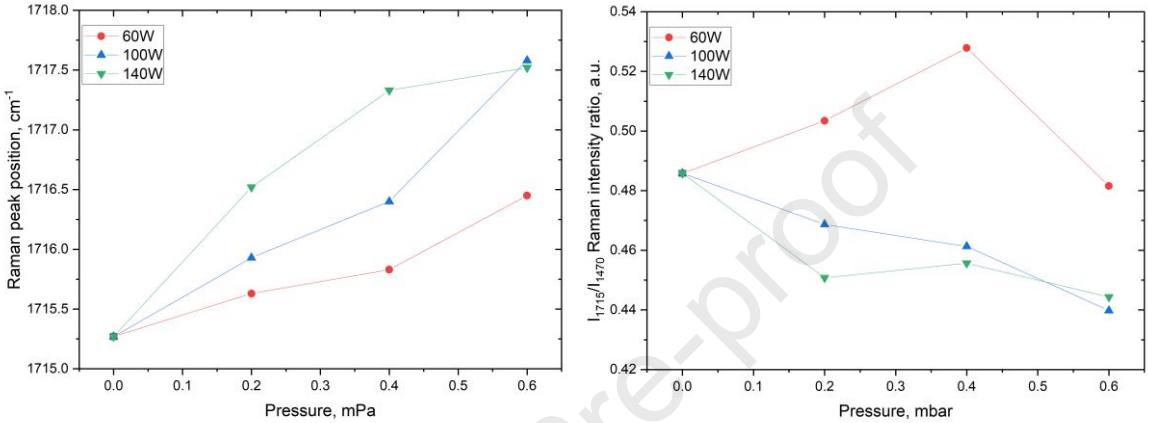

Figure 19 *Change of the position (left) and the relative intensity (right) of the 1715 cm^{-1} Raman peak with plasma pressure for different powers.*

4. Conclusions

The rate and effect of low-pressure oxygen plasma etching of a UDMA:TEGDMA 3:1 polymer mixture were investigated for various plasma etching settings. It was shown that by controlling the power and pressure parameters, steady etching rates in the 0.11 – 0.48 μm/min range can be reached. The relationship between the etching time and the increase of the surface roughness was discussed: as the former increases, the changes in the latter affect the etching rate and also cause a decrease in optical transparency. It was also pointed out that in the case of plasma etching the applied pressure and the surface roughness are in an inverse relationship in the investigated parameter range. Correlating these results with the internal plasma parameters obtained by actinometry showed that both the etching rate and the surface roughness correlates well with the O density in the applied plasmas, indicating the dominance of reactive neutral density in these processes. It was also shown with Raman spectroscopy that etching the polymer with oxygen plasma causes minor structural changes in the polymer matrix, including the level of crosslinking and internal stress, as well as breakdown or removal of the EDAB co-initiator molecules entrapped in the structure.

Acknowledgements

Project no. C1014183 has been implemented with the support provided by the Ministry of Culture and Innovation of Hungary from the National Research, Development and Innovation Fund, financed under the KDP-2020 funding scheme.

This work was partially supported by Nanoplasmonic Laser Fusion Research Laboratory project financed by the National Research and Innovation Office (2022-2.1.1-NL-2022-00002), Hungary.

Data Availability Statement

The data is available from the authors upon request.

References

1. Asmussen, E., & Peutzfeldt, A. (1998). Influence of UEDMA, BisGMA and TEGDMA on selected mechanical properties of experimental resin composites. *Dental Materials*, *14*(1), 51–56. https://doi.org/10.1016/S0109-5641(98)00009-8

2. Davy, K. W. M., Kalachandra, S., Pandain, M. S., & Braden, M. (1998). Relationship between composite matrix molecular structure and properties. *Biomaterials*, *19*(22), 2007–2014. https://doi.org/10.1016/S0142-9612(98)00047-7

3. Kalachandra, S., Taylor, D. F., DePorter, C. D., Grubbs, H. J., & McGrath, J. E. (1993). Polymeric materials for composite matrices in biological environments. *Polymer*, *34*(4), 778–782. https://doi.org/10.1016/0032-3861(93)90363-F

4. Pratap, B., Gupta, R. K., Bhardwaj, B., & Nag, M. (2019). Resin based restorative dental materials: characteristics and future perspectives. *Japanese Dental Science Review*, *55*(1), 126–138. https://doi.org/10.1016/j.jdsr.2019.09.004

5. Bukovinszky, K., Szalóki, M., Csarnovics, I., Bonyár, A., Petrik, P., Kalas, B., … Hegedűs, C. (2021). Optimization of Plasmonic Gold Nanoparticle Concentration in Green LED Light Active Dental Photopolymer. *Polymers*, *13*(2), 275. https://doi.org/10.3390/polym13020275

6. Elsubeihi, E. S., Aljafarawi, T., & Elsubeihi, H. E. (2020). State of the Art Contemporary Prefabricated Fiber-Reinforced Posts. *The Open Dentistry Journal*, *14*(1), 313–323. https://doi.org/10.2174/1874210602014010313

7. Alshabib, A., Abid Althaqafi, K., AlMoharib, H. S., Mirah, M., AlFawaz, Y. F., & Algamaiah, H. (2023). Dental Fiber-Post Systems: An In-Depth Review of Their Evolution, Current Practice and Future Directions. *Bioengineering*, *10*(5), 551. https://doi.org/10.3390/bioengineering10050551

8. ROPERTO, R. C., PORTO, T. S., LANG, L., TEICH, S., WEBER, S., EL-MOWAFY, O., & PORTO-NETO, S. T. (2016). Microtensile bond strength between a UDMA fiber post and different resin cements: Effect of pre-surface treatment. *Dental Materials Journal*, *35*(6), 923–928. https://doi.org/10.4012/dmj.2016-034

9. YAVIRACH, P., CHAIJAREENONT, P., BOONYAWAN, D., PATTAMAPUN, K., TUNMA, S., TAKAHASHI, H., & ARKSORNNUKIT, M. (2009). Effects of plasma treatment on the shear bond strength between fiber-reinforced composite posts and resin composite for core build-up. *Dental Materials Journal*, *28*(6), 686–682. https://doi.org/10.4012/dmj.28.686

10. Costa Dantas, M. C., do Prado, M., Costa, V. S., Gaiotte, M. G., Simão, R. A., & Bastian, F. L. (2012). Comparison between the Effect of Plasma and Chemical Treatments on Fiber Post Surface. *Journal of Endodontics*, *38*(2), 215–218. https://doi.org/10.1016/j.joen.2011.10.020

11. Wei, Q. F., Gao, W. D., Hou, D. Y., & Wang, X. Q. (2005). Surface modification of polymer nanofibres by plasma treatment. *Applied Surface Science*, *245*(1–4), 16–20. https://doi.org/10.1016/j.apsusc.2004.10.013

12. Cvelbar, U., Pejovnik, S., Mozetiè, M., & Zalar, A. (2003). Increased surface roughness by oxygen plasma treatment of graphite/polymer composite. *Applied Surface Science*, *210*(3–4), 255–261. https://doi.org/10.1016/S0169-4332(02)01286-2

13. Vesnel, A., & Semenic, T. (2012). Etching Rates of Different Polymers in Oxygen Plasma. *Materiali in Tehnologije*, *46*, 227–231.

14. Vourdas, N., Boudouvis, A. G., & Gogolides, E. (2005). Plasma etch rate measurements of thin PMMA films and correlation with the glass transition temperature. *Journal of Physics: Conference Series*, *10*, 405–408. https://doi.org/10.1088/1742-6596/10/1/099

15. Shimomukai, K., Kawata, H., Yasuda, M., & Hirai, Y. (2015). High Selective Plasma Etching of PMMA to PS. *Journal of Photopolymer Science and Technology*, *28*(4), 569–572. https://doi.org/10.2494/photopolymer.28.569

16. Yamamoto, H., Imamura, T., Omura, M., Sakai, I., & Hayashi, H. (2014). Selective etch of poly(methyl methacrylate) in block copolymer based on control of ion energy and design of gas chemistry for directed self assembly lithography. *Japanese Journal of Applied Physics*, *53*(3S2), 03DD03. https://doi.org/10.7567/JJAP.53.03DD03

17. Imamura, T., Yamamoto, H., Omura, M., Sakai, I., & Hayashi, H. (2015). Highly selective removal of poly(methyl methacrylate) from polystyrene- *block* -poly(methyl methacrylate) by CO/H2 plasma etching. *Journal of Vacuum Science & Technology B, Nanotechnology and Microelectronics: Materials, Processing, Measurement, and Phenomena*, *33*(6). https://doi.org/10.1116/1.4932541

18. Fricke, K., Steffen, H., von Woedtke, T., Schröder, K., & Weltmann, K. (2011). High Rate Etching of Polymers by Means of an Atmospheric Pressure Plasma Jet. *Plasma Processes and Polymers*, *8*(1), 51–58. https://doi.org/10.1002/ppap.201000093

19. Choi, P., Fu, P. -F., & Guo, L. J. (2007). Siloxane Copolymers for Nanoimprint Lithography. *Advanced Functional Materials*, *17*(1), 65–70. https://doi.org/10.1002/adfm.200600257

20. Huang, R., & Weigand, M. (2008). Plasma etch properties of organic BARCs. In C. L. Henderson (Ed.), (p. 69232G). https://doi.org/10.1117/12.772012

21. May, M. J., Mortini, B., Heitzmann, M., Gautier, P., Sourd, C., Brochon, C., & Hadziioannou, G. (2006). Investigating 248 and 193nm resist degradation during reactive ion oxide etching. *Microelectronic Engineering*, *83*(4–9), 1098–1102. https://doi.org/10.1016/j.mee.2006.01.169

22. Zahid, M. A., Park, H., Cho, Y. H., & Yi, J. (2021). Plasma etched PMMA/CaF2 anti-reflection coating for light weight PV module. *Optical Materials*, *112*, 110813. https://doi.org/10.1016/j.optmat.2021.110813

23. Di Mundo, R., Troia, M., Palumbo, F., Trotta, M., & d'Agostino, R. (2012). Nano-texturing of Transparent Polymers with Plasma Etching: Tailoring Topography for a Low Reflectivity. *Plasma Processes and Polymers*, *9*(10), 947–954. https://doi.org/10.1002/ppap.201200041

24. Borok, A., Gal, D., Kovacs, R., Szokol, A. N., & Bonyar, A. (2022). Investigation of Plasma Etching Rates of a Methacrylate Resin. In *2022 45th International Spring Seminar on Electronics Technology (ISSE)* (pp. 1–5). IEEE. https://doi.org/10.1109/ISSE54558.2022.9812707

25. M. Hori, "Radical-controlled plasma processes," Rev. Mod. Plasma Phys. 2022 61, vol. 6, no. 1, pp. 1–117, Nov. 2022, doi: 10.1007/S41614-022-00084-2.

26. R. Miotk, B. Hrycak, M. Jasiński, and J. Mizeraczyk, "Characterization of an Atmospheric-Pressure Argon Plasma Generated by 915 MHz Microwaves Using Optical Emission Spectroscopy," J. Spectrosc., vol. 2017, no. 1, p. 6359107, Jan. 2017, doi: 10.1155/2017/6359107

27. M. Fiebrandt, N. Bibinov, and P. Awakowicz, "Determination of atomic oxygen state densities in a double inductively coupled plasma using optical emission and absorption spectroscopy and probe measurements," Plasma Sources Sci. Technol., vol. 29, no. 4, Apr. 2020, doi: 10.1088/1361-6595/AB7CBE

28. Y. Wang, J. Chen, Y. Wang, and W. Xiong, "The influence of oxygen ratio on the plasma parameters of argon RF inductively coupled discharge," Vacuum, vol. 149, pp. 291–296, Mar. 2018, doi: 10.1016/j.vacuum.2018.01.008

29. Masruroh, D. J. D. H. Santjojo, Abdurrouf, M. A. Abdillah, M. C. Padaga, and S. P. Sakti, "Effect of Electron Density and Temperature in Oxygen Plasma Treatment of Polystyrene Surface," IOP Conf. Ser. Mater. Sci. Eng., vol. 515, no. 1, 2019, doi: 10.1088/1757-899X/515/1/012061

30. N. Britun, M. K. T. Mo, S. N. Hsiao, F. J. T. Arellano, M. Sekine, and M. Hori, "Optical actinometry for number density measurements in low-pressure plasmas: Advantages, error sources, and method validation," J. Appl. Phys., vol. 136, no. 11, p. 111101, Sep. 2024, doi: 10.1063/5.0227576/3313170

31. N. C. M. Fuller, M. V. Malyshev, V. M. Donnelly, and I. P. Herman, "Characterization of transformer coupled oxygen plasmas by trace rare gases-optical emission spectroscopy and Langmuir probe analysis," Plasma Sources Sci. Technol., vol. 9, no. 2, pp. 116–127, May 2000, doi: 10.1088/0963-0252/9/2/304

32. D. V. Lopaev, A. V. Volynets, S. M. Zyryanov, A. I. Zotovich, and A. T. Rakhimov, "Actinometry of O, N and F atoms," J. Phys. D. Appl. Phys., vol. 50, no. 7, p. 075202, Jan. 2017, doi: 10.1088/1361-6463/50/7/075202

33. C. E. Schäfer et al., “Comparative study of electron temperature and ion energy in two different magnetic nozzle thruster designs,” J. Electr. Propuls., vol. 3, no. 1, pp. 1–20, Dec. 2024, doi: 10.1007/S44205-024-00094-X/FIGURES/8

34. Bonyár, A., Szalóki, M., Borók, A., Rigó, I., Kámán, J., Zangana, S., … Kroó, N. (2022). The Effect of Femtosecond Laser Irradiation and Plasmon Field on the Degree of Conversion of a UDMA-TEGDMA Copolymer Nanocomposite Doped with Gold Nanorods. *International Journal of Molecular Sciences*, *23*(21), 13575. https://doi.org/10.3390/ijms232113575

35. Socrates, G. (2004). *Infrared and Raman Characteristic Group Frequencies: Tables and Charts* (Third.). John Wiley & Sons.

36. BinMahfooz AM, Qutub OA, Marghalani TY, Ayad MF, Maghrabi AA. Degree of conversion of resin cement with varying methacrylate compositions used to cement fiber dowels: A Raman spectroscopy study. J Prosthet Dent. 119 (2018) 1014-1020. doi: 10.1016/j.prosdent.2017.09.002

37. Mahmood MH, Himics L, Váczi T, Rigó I, Holomb R, Beiler B, Veres M., Raman spectroscopic study of gamma radiation-initiated polymerization of diethylene glycol dimethacrylate in different solvents, Journal of Raman Spectroscopy 52 (2021) 1735-1743. doi: https://doi.org/10.1002/jrs.6207

38. K. Yamada et al., “Foundations of plasma surface functionalization of polymers for industrial and biological applications,” Plasma Sources Sci. Technol., vol. 31, no. 10, p. 103001, Oct. 2022, doi: 10.1088/1361-6595/AC70F9

39. M. Satake, T. Iwase, M. Kurihara, N. Negishi, Y. Tada, and H. Yoshida, “Effect of oxygen addition to an argon plasma on etching selectivity of poly(methyl methacrylate) to polystyrene,” Journal of Micro/Nanolithography, MEMS, and MOEMS, vol. 12, no. 4, p. 041309, Nov. 2013, doi: 10.1117/1.JMM.12.4.041309.

40. U. Cvelbar, S. Pejovnik, M. Mozetiè, and A. Zalar, “Increased surface roughness by oxygen plasma treatment of graphite/polymer composite,” Appl. Surf. Sci., vol. 210, no. 3–4, pp. 255–261, Apr. 2003.

41. J.-P. Booth, M. Mozetič, A. Nikiforov, and C. Oehr, “Foundations of plasma surface functionalization of polymers for industrial and biological applications,” Plasma Sources Sci. Technol., vol. 31, no. 10, p. 103001, Oct. 2022, doi: 10.1088/1361-6595/ac70f9.doi: 10.1016/S0169-4332(02)01286-2.

42. E. Gogolides et al., “Controlling roughness: from etching to nanotexturing and plasma-directed organization on organic and inorganic materials,” J. Phys. D. Appl. Phys., vol. 44, no. 17, p. 174021, May 2011, doi: 10.1088/0022-3727/44/17/174021.

Highlights

The effect of low-pressure oxygen plasma etching on the physical properties of UDMA:TEGDMA in 3:1 weight ratio was investigated.

By controlling the power and pressure parameters, steady etching rates can be set up in the 0.11 – 0.48 mm/min range.

Etching times above one hour increased the surface roughness of the polymer significantly, while reduced its optical transparency.

This loss in transparency was successfully restored by depositing a second polymer layer on top of the plasma-etched one.

Raman spectroscopy showed that the degree of conversion and the amount of aromatic molecules were influenced by the etching.

Declaration of interests

☒ The authors declare that they have no known competing financial interests or personal relationships that could have appeared to influence the work reported in this paper.

☐ The authors declare the following financial interests/personal relationships which may be considered as potential competing interests: